

## EXPERIMENTAL STUDY AND PORE-SCALE NUMERICAL MODELING OF PERMEABILITY IMPAIRMENT RESULTING FROM ASPHALTENE PRECIPITATION IN POROUS MEDIUM

Abbas Khaksar Manshad<sup>1,5\*</sup>, Rouhollah Fatehi<sup>2</sup>, Amir H. Mohammadi<sup>3\*</sup>, Jagar A. Ali<sup>5</sup>, Siavash Ashoori<sup>4</sup>, Rasoul Hassanalizadeh<sup>3</sup>

<sup>1</sup> Department of Petroleum Engineering, Abadan Faculty of Petroleum Engineering, Petroleum University of Technology (PUT), Abadan, Iran

<sup>2</sup> Department of Mechanical Engineering, School of Engineering, Persian Gulf University, Bushehr, Iran

<sup>3</sup> Discipline of Chemical Engineering, School of Engineering, University of KwaZulu-Natal, Howard College Campus, Durban 4041, South Africa

<sup>4</sup> Department of Petroleum Engineering, Ahwaz Faculty of Petroleum Engineering, Petroleum University of Technology (PUT), Ahwaz, Iran

<sup>5</sup> Department of Petroleum Engineering, Faculty of Engineering, Soran University, Kurdistan Region- Iraq

Received February 7, 2018; Accepted April 23, 2018

---

### Abstract

Asphaltene precipitation affects the formation by reducing the porosity and permeability. In this study the permeability reduction asphaltene precipitation in granular porous media has been modeled using pore-scale simulation. In this way, the pore-scale geometry of a granular porous medium is used, and governing equations are solved numerically by an improved version of weakly compressible Smoothed Particle Hydrodynamics (SPH). Based on the results of the pore-scale simulation, a model is proposed for the permeability change of a single cell (grain) in the porous media. In this model, there are two parameters; final to initial permeability and characteristics time of precipitation that are evaluated through pore-scale simulation. Then, the proposed model is averaged through an up-scaling process to lead to a macro-scale relation which independently of the changes in the porosity predicts the time evolution of the permeability reduction. Experimental procedure has been conducted in a synthetic porous medium made of the slim tube, which was filled with glassy beds. Different flood tests were carried out at different temperatures and injection rates to test the volume ratio of oil to solvent. A predictive model has been developed to assess the permeability reduction via asphaltene precipitation. The main assumption for the model is based on the theory of deep bed filtration and the relationship between damaged and initial permeability, which is a function of the porosity change with asphaltene deposition. The developed model simulates the permeability reduction in flooding tests using computer code. The model provides good fit from the experimental data, which is an indication of the reliability of the developed model.

**Keywords:** Permeability Impairment; Asphaltene Precipitation; Porous Media; Smoothed particle Hydrodynamics; Model.

---

## 1. Introduction

Asphaltene is a mixture of a set of hydrocarbon(s) that can precipitate at different reservoir conditions. After starting the precipitation, the fine particles aggregate. The mentioned process is reversible which allows the collected particles to dissociate and make the initial fine particles. Rock surface is capable of adsorbing and trapping the aggregates on their pores, which depends on the size of the porous media (plugging). Due to high local velocity known as shear, it can be returned into the oil phase. Effective mobility of hydrocarbon can be reduced with asphaltene by:

- a) Reducing the permeability of the rock by blocking the pore throats,
- b) Changing the formation wettability started with adsorption to rock surface, which diminishes the permeability and increases the oil saturation as it cannot be reduced again.
- c) Forming an ionized solution (colloidal) in the oil phase, which increases the viscosity of the reservoir fluid.

Asphaltene precipitation reduces the porosity. Correlating the porosity reduction to the rock permeability declination can be considered using power law relationship. The power law relationship gives the ratio of the permeability  $K$  to the initial permeability  $K_{init}$  at time  $t$ , e.g., in the way used by Civan [1].

When asphaltene forms without water and under saturated oil, the permeability declination is the main mechanism of damage. The radius of damage depends on the draw down, and it occurs deep in the reservoir. There are plenty of developed models for the precipitation of the asphaltene in core tests. Civan [2-3] categorized flow channels of porous media into the groups of plugging and non-plugging trajectories. For the modelling, pore throat plugging of surface adsorption and dragging the precipitates are considered.

Ali and Islam [4] assumed the suspension of asphaltene in crude oil, which is ready to precipitate. Further factors of the model include entrainment of the deposits and surface adsorption. Wang *et al.* [5-6] used ideal solution theory to simulate deposition process. Two factors to model the asphaltene deposition are plugging of the surface adsorption and entrainment.

In this study, a numerical model has been developed to predict a reduction of permeability due to asphaltene precipitation. To this end, pore scale geometry of a granular porous medium is used, and governing equations are solved numerically, which is Smoothed Particle Hydrodynamics (SPH). This method is not applying the Lagrangian mesh, which makes it a popular method of computational fluid dynamics (CFD) modelling approaches. It is easy to implement and flexible while handling large displacements and interfaces of complex fluids. Lucy [7] and Gingold and Monaghan [8] initially developed the SPH method in the same time for simulating astrophysical problems which was extended to many fields of fluid flows and solid mechanics [9].

In this work, an improved version of weakly compressible SPH was used as suggested in recent work of Fatehi and Manzari [10]. This improvement includes more consistent scheme for discretization of second derivatives in conjunction with a numerical filter for reduction of non-physical oscillations and a new method for implementation of wall boundary condition. Another novelty of this work is that in contrast with the common models in the literature the model proposed to predict the time evolution of the permeability inclination is independent of the changes in the porosity.

In the following, first, the phenomenon is studied in pore-scale. The computational domain governing equations and the numerical method are described, and the obtained results are presented. In the next section, based on the results of pore-scale simulation a model is proposed for the permeability change of a single cell (grain) in the porous media. Then, the proposed model is averaged through an up-scaling process to lead to a relation for the permeability reduction due to asphaltene precipitation in a slim tube.

## 2. Experiments of the slim tube

### 2.1. Material and equipment

Table 1 shows properties of the target crude oil which were taken from an oil field in the Southern part of Iran. It is heavy oil (relatively) which has a gravity index equal to 20° API with asphaltene content of 11 weight percent. The sample (crude oil) was kept at specific laboratory conditions (almost three months) to eliminate the volatile components and reach to a fixed composition for the equilibrium condition. In association with oil production, further, than oil, there are possible contaminations such as sand and clay. Hence, Whatman paper filter (number 42) was applied to eliminate the mentioned impurities. In our gravimetric experimental method, n-heptane was taken as the precipitant to measure the quantity of the deposited asphaltene.

Several experiments were conducted on the porous medium (the synthetic medium) at high temperature and pressure (reservoir condition) to study the asphaltene deposition phenomenon. Figure 1 shows the experimental apparatus. It consists of a slim tube submerged in an oil bath, vacuum and liquid pumps, a transparent capillary tube connected to a heating jacket, which helps to monitor the fluid flow, a pressure regulator for resulting oil, a container to collect the final oil, and connected pressure gauges.

Table 1. Composition and characteristics of the crude oil [13-15, 17]

Component	Mole %	Property	Value
H <sub>2</sub> S	0.192	Reservoir Oil MW (g/gmol)	156.67
Nitrogen	0	Test temperature (F)	225
CO <sub>2</sub>	2.204	MW C <sub>7+</sub> (g/gmol)	316.49
Methane	26.945	SG C <sub>7+</sub>	0.9272
Ethane	8.008	Density of reservoir fluid @ Pb (g/cc)	0.7646
Propane	6.426	Bubble point pressure (psia)	1890
i-Butane	1.134	Asphaltene content in stock tank oil, wt%	11
n-Butane	3.682		
i-Pentane	1.742		
n-Pentane	2.233		
Hexanes	4.202		
Heptanes+	43.212		

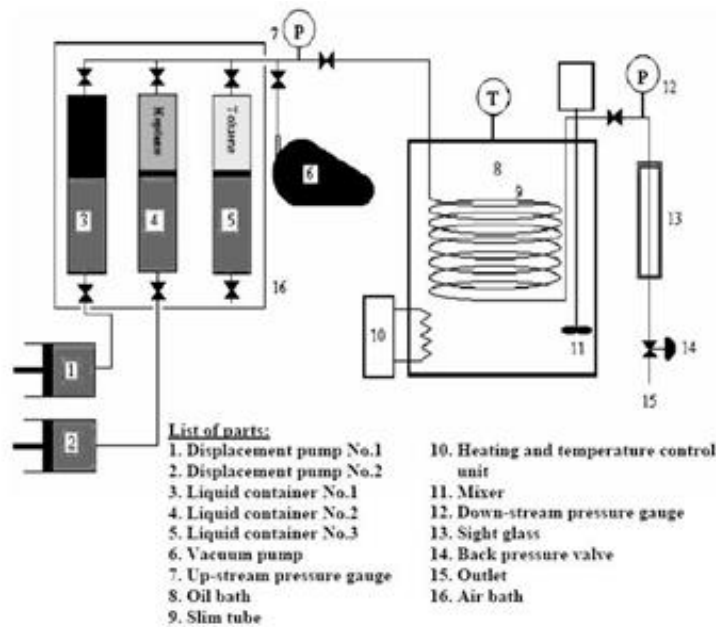


Figure 1. A schematic diagram of the experimental setup [14-16]

A Ruska tube was used to measure the quantity of the lost permeability resulting from asphaltene deposition in the porous medium. The tube is made of stainless steel tube coil with outside diameter and inside diameter of 7.9 and 6.2 mm, respectively with the length of 18.3 m. The tube is coiled (up to 20 cm of diameter). Small round glass beds of 150-170 micrometre are used to pack the slim column.

The porosity of the porous medium is almost 27 % with an approximate absolute permeability of  $4.93 \times 10^{-12} \text{ m}^2$  (5 Darcies). The total approximate volume of the available voids is 150 cm<sup>3</sup>.

The isothermal oil bath can be heated up to 175°C using a heat insulated tank which is controlled thermostatically with an approximate volume of 60 liters. The circulating mixer and heating element are mounted by a duct which leads to the full circulation of the fluid inside the bath. It is equipped with a temperature controller with 1°C resolution. The tube is placed

vertically, and the inlet valve and outlet valve are located on top side of the temperature bath. To distribute the temperature evenly, the tube is submerged fully into the bath. The transparent high pressure tube is located at the end of the slim tube (downstream). The passing fluid can be either one phase or two-phase slug flow.

Two pressure gauges are connected to the tube with the aim to monitor the pressure of the upstream and downstream which is controlled using a backpressure regulator connected to the downstream side after flushing the resulting oil to the atmospheric condition.

There are two cylinder-pistons of 500 m<sup>3</sup> volume inside the pump with a variable flow rate of 1 to 1999 cm<sup>3</sup>/hr. The accuracy of the pump is 0.0025 cm<sup>3</sup> using a calibrated ruler which can work up to 70 MPa and controlled by computer and manual as well.

## **2.2. Experimental technique**

The two categories of the experimental technique are as follows:

### **2.2.1. Initial activities**

The initial activities include:

- a. To wash the slim Rusk tube
- b. To dry the tube
- c. To evacuate the tube
- d. To fill the vessel of fluid transfer
- e. To measure the pore volume
- f. To study the system in terms of flow behavior
- g. To measure the permeability
- h. To calculate the porosity of packed bed using the equation of Carman-Kozeny.

### **2.2.2. Flooding experiments**

The effect of injection rate, temperature, and solvent to oil ratio on permeability declination (resulted from asphaltene deposition) were studied by conduction several flooding experiments and considering the factor of time. The calculated Reynolds number for injection rate was less than unity, which leads to Darcy's law as a method to obtain the permeability.

Initial activities were conducted to find the operational condition of the flooding tests on the porous medium. The flood test procedure is as follows:

1. The filtered crude oil is filled to one of the vessels of fluid transfer and n-heptane to the other one.
2. The fluid transfer vessels are connected with a line to each other from top valves of the vessels using a T-junction between them.
3. Each vessels bottom is connected to a pump which is set to the flow rate that is desired and evacuated to eliminate the possible impurities such as air.
4. The porous medium is then connected to the T-injection outlet of the evacuated vessel.
5. Fluids are injected to mix the n-heptane with crude oil. The pump is activated at the same time that the porous medium's inlet valve is opened with recording the initial time.
6. Internal pressure to the porous medium is monitored and recorded every 2 minutes. The mixture of the n-heptane and crude oil passes through the porous medium. After filling the medium with the volume of one pore (150 cm<sup>3</sup>) of the mixture, the entrance pressure starts to increase. The exit valve is opened to produce the mixture consequently. The inlet pressure drops and in a short time reaches a steady state condition. Increasing the pressure is the reason that shows asphaltene precipitates. After observing the product at the outlet valve, it is necessary to take a sample after every 10 minutes. Continues sampling process stops after injection of at least 4 times of pore volume to the tube. The highest allowed pressure to avoid safety problems is 28 MPa.
7. The obtained samples are used to obtain the deposited asphaltene, which leaves the tube and remains in the taken samples.

Either the porous medium permeability versus time or injected fluid pore volume can be calculated using Darcy’s law as well as the obtained data from the step 6. This experiment can show the effect of different factors on severity of the damage due to permeability reduction. Measured data at the 7<sup>th</sup> step shows the concentration of the deposited asphaltene with varying time. Table 2 reports the conditions for these experiments.

**3. Pore-Scale simulation**

To predict the behavior of the porous media in asphaltene precipitation process a pore scale model of a two-dimensional granular porous medium (as shown in Figure 2) is considered. It is constructed from similar circular cylinders all of diameter *D* which are infinitely placed in a regular inline arrangement. Here, the spacing in both transversal and longitudinal directions is equal *S*.



Figure 2. Schematic of the regular granular medium used here for pore-scale simulations

Initially, the medium is filled with an oil free from asphaltene particles at the time *t*=0 another heavy oil with precipitated asphaltene flocs of concentration *C<sub>i</sub>* is injected from the right hand boundary. This causes the whole fluid in the medium to flow from right to left. As the asphaltene flocs approach to the low speed regions near the grains they merge and form deposits attached to the solid walls. This leads to two consequences; first, the cross section area of the fluid flow is reduced which means a reduction in porosity and permeability of the medium. The other consequent of asphaltene precipitation is that the fluid flows in the remaining area more rapidly providing the flow rate be constant. This increase in velocity prevents more asphaltene particles from settling. Precipitation of particles first occurs at the first grain, and then it promotes in the way of the flow to the next grains.

**3.1. Governing equations**

Here, mass and momentum conservations are applied. Since the numerical method (SPH) uses the Lagrangian approach, the conservation equations are written in the Lagrangian form. For the solution, mass conservation is

$$\frac{d\rho}{dt} = -\rho \nabla y \tag{1}$$

In addition, momentum conservation assuming Newtonian fluid and incompressible flow leads to

$$\rho \frac{dv}{dt} = -\frac{1}{\rho} \nabla P + \mu \nabla^2 v + \rho g \quad (2)$$

Here,  $\mu$  and  $\rho$  denote viscosity and density of the solution, respectively.

In addition,  $V$  and  $P$  are velocity vector and pressure, respectively. For the concentration of asphaltene flocs, one can write a transport equation like

$$\frac{dC}{dt} = D \nabla^2 C \quad (3)$$

where,  $C$  is a concentration of precipitated asphaltene flocs in mole/m<sup>3</sup> and  $D$  is diffusion coefficient.

Since asphaltene precipitates and forms into flocs; this diffusion cannot be Fickian or molecular diffusion. However, in practice, there is always diffusion effect due to the Brownian motion of particles and other possible effects.

### 3.2. Numerical method

To solve the governing equations based on numerical methods, as mentioned earlier, a Lagrangian method known as SPH is used. In this section, general discretization plans for the first spatial derivatives and second spatial derivatives of field values and boundary conditions adopted for this problem are introduced. More details of discretization and solution algorithm for a discrete form of governing equations (1) to (3) can be found in reference [10].

#### 3.2.1. SPH formulation

The SPH method is based on the interpolation concept. For a random function of the field such as  $u$ , the value, which is interpolated ( $u$ ) for the neighboring particles values  $u_j$ , can be calculated using the following equation:

$$(u(r)) = \sum_j \omega_j u_j W(r - r_j, h) \quad (4)$$

where,  $\omega_j$  denotes the volume or weight of particle  $j$ ,  $r$  denotes the position vector,  $W$  denotes the kernel or smoothing function and  $h$  denotes the circular compact support radius.

Here, the quantic Wendland function [11] is used. For obtaining the first derivative's numerical approximation ( $u$ )<sub>*i*</sub> the following equation can be used [12]:

$$(\nabla u)_i = \sum_j \omega_j B_i \cdot \nabla W_{ij} (u_j - u_i) \quad (5)$$

where,  $W_{ij} = W(r_i - r_j, h)$  is the value of smoothing or kernel function of particle  $i$  at the position of particle  $j$ . Also,

$$B_i = -[\omega_j r_{ij} \nabla W_{ij}]^{-1} \quad (6)$$

is a renormalization tensor in which  $r_{ij} = r_i - r_j$  shows the distance of  $i$  and  $j$  particles. For the second derivative, a consistent scheme is used,

$$(\Delta \cdot \nabla u)_i = \hat{B}_i : \sum_j 2\omega_j e_{ij} \nabla W_{ij} \left( \frac{u_i - u_j}{r_{ij}} - e_{ij} \cdot \sum_j \omega_j (u_i - u_j) B_i \nabla W_{ij} \right) \quad (7)$$

where  $r_{ij} = |r_{ij}|$  and  $e_{ij} = \hat{r}_{ij}/r_{ij}$  is a unit vector in the direction of inter-particle.

It is noticeable that ( $u$ ) is calculated as in Eq. (5) and  $B$  is a new renormalisation tensor for the second derivative calculated by

$$\hat{B}_i : [\sum_j \omega_j r_{ij} e_{ij} e_{ij} \nabla W_{ij} + (\sum_j \omega_j e_{ij} e_{ij} \nabla W_{ij}) \cdot B_i (\sum_j \omega_j r_{ij} r_{ij} \nabla W_{ij})] = -1 \quad (8)$$

#### 3.2.2. Boundary conditions

Since the domain is geometrically periodic and the Reynolds' number of the flow is very small, the modified pressure and velocity  $\tilde{P} = P + \rho g x$  of the domain can be treated using some finite number of solid grains with periodic boundary conditions on all outer boundaries. Figure 3 shows a sample of the computational domain. In this figure, also the initial arrangement of SPH particles can be seen. Here, dark dots are fluid particles and lights are solid particles, which represent the wall boundaries of grains.

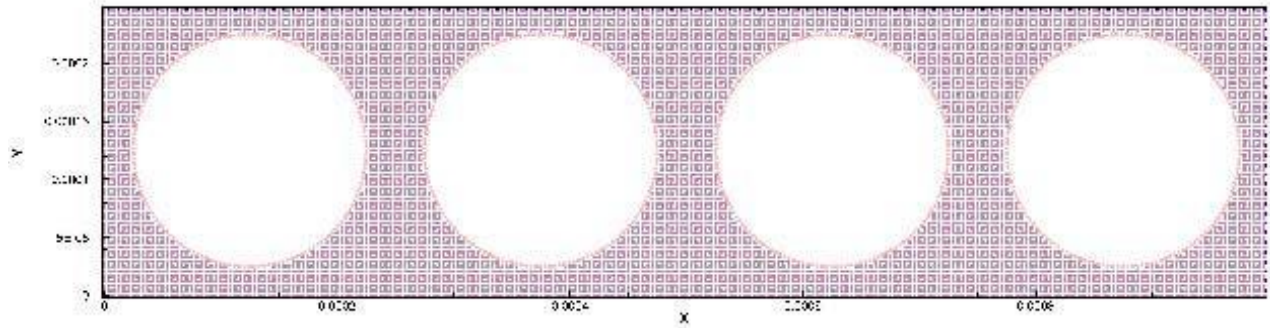


Figure 3. A Sample of computational domain with initial arrangement of SPH particles. All outer boundaries (solid lines) are treated as periodic boundary conditions in mass and momentum equations

Each SPH particle exiting the right-hand boundary enters at the corresponding point from the left boundary with the same properties including velocity and modified pressure. However, this condition cannot be applied for the concentration of asphaltene flocs  $C$ . The entering SPH particles from the left boundary necessarily bring the particular amount of asphaltene flocs  $C_n$  that is defined using the thermodynamic properties of the injected heavy oil.

### 3.2.3. Wall boundaries and precipitation

In the momentum equation (2), the surfaces of grains are treated as a no-slip condition. Since the velocity of the fluid particles is similar to the wall, consequently their acceleration is equal to zero. Then we have:

$$\frac{\nabla P}{\rho} \cdot n = g \cdot n \tag{9}$$

where  $n$  denotes the unit vector.

The unit vector is normal to the wall, which is obtained by summing the kernel gradients. It can be shown as follow:

$$n_i = \frac{\sum_j \omega_j \nabla W_{ij}}{|\sum_j \omega_j \nabla W_{ij}|} \tag{10}$$

Hence, assuming the location of particle  $i$  on the wall, one can conclude that its velocity is apparent (that would be zero for the fixed wall) and the pressure for the next step ( $P_i^{n+1}$ ) can be found from,

$$P_i^{n+1} = \frac{\left(\sum_j \omega_j \frac{P_j^{n+1}}{\rho_{ij}} B \cdot \nabla W_{ij}\right) \cdot n_i - g \cdot n_i}{\left(\sum_j \omega_j \frac{1}{\rho_{ij}} B \cdot \nabla W_{ij}\right) \cdot n_i} \tag{11}$$

here  $j$  denotes all particles in the neighboring of particle  $i$ , which includes the particles on the wall.

Thus, calculation of the new time-step pressure  $P^{n+1}$  needs a limited number of iteration (i.e., 3 iterations) with wall particles [10]. When an asphaltene floc approaches the walls of the grains, it may settle down depending on its velocity and concentration of asphaltene near the wall. Here, precipitation of asphaltene floc in the porous medium is simulated using some rules. An SPH particle deposits on the wall provided that:

- Its asphaltene concentration  $C$  is higher than a critical value  $C_{cr}$ ;
- The distance to the nearest particle on a wall or a deposited SPH particle is less than  $h$ ;
- Its velocity magnitude  $V$  is less than a critical value  $V_{cr}$ .

After a particle was deposited, its velocity is set to zero, and the viscosity is enlarged by ten times to better simulate the properties of the deposits.

## 4. Numerical results

The aforementioned problem was solved numerically using the SPH method described in the previous section. Physical properties and numerical parameters of the problem are summarized in table 3 where Courant number is defined as  $C_r = c\Delta x/\Delta t$  in which  $\Delta x$  and  $\Delta t$  are

initial spacing between SPH particles and time-step size, respectively. In this case, using  $\Delta x = 4.17 \times 10^{-6}$  m leads to approximately 7700 SPH particles. The initial arrangement of particles is illustrated in Figure 3. The kernel function for smoothing radius ( $h$ ) is selected as  $2.5 \Delta x$  in this simulation, which for each particle; it is equivalent to approximately 20 neighbors.

Table 3. Physical properties and numerical parameters of the simulated problem

Parameter	Symbol	Value	Unit
Diameter of grains	D	$2.0 \times 10^{-4}$	m
Grains spacing	S	$2.5 \times 10^{-4}$	m
Fluid's density	$\rho$	$10^{-3}$	kg/m <sup>3</sup>
Fluid's viscosity	$\mu$	$10^{-3}$	Pa.s
Diffusion coefficient	$\mathcal{D}$	$10^{-7}$	mm <sup>2</sup> /s
Body force acceleration	G	$10^{-2}$	m/s <sup>2</sup>
Critical velocity	$V_{\sigma}$	$2.0 \times 10^{-4}$	m/s
Artificial speed of sound	C	0.2	m/s
Courant number	Cr	0.3	-

The obtained results of asphaltene flocs concentration are shown in Figure 4. In this figure, the contour plot of the fraction of asphaltene flocs concentration  $C$  to the inlet value  $C_{in}$  is illustrated for six different times after injection. In early times, two channels are formed up and down the grain, and the fluid preferred to flow through these channels. Thus, the domain can be divided into high-speed regions, i.e., these channels and low-speed regions which include the spaces between the grains in the middle of the domain horizontally. In high-speed regions, the dominant effect is advection while in the latter diffusion effect is more significant.

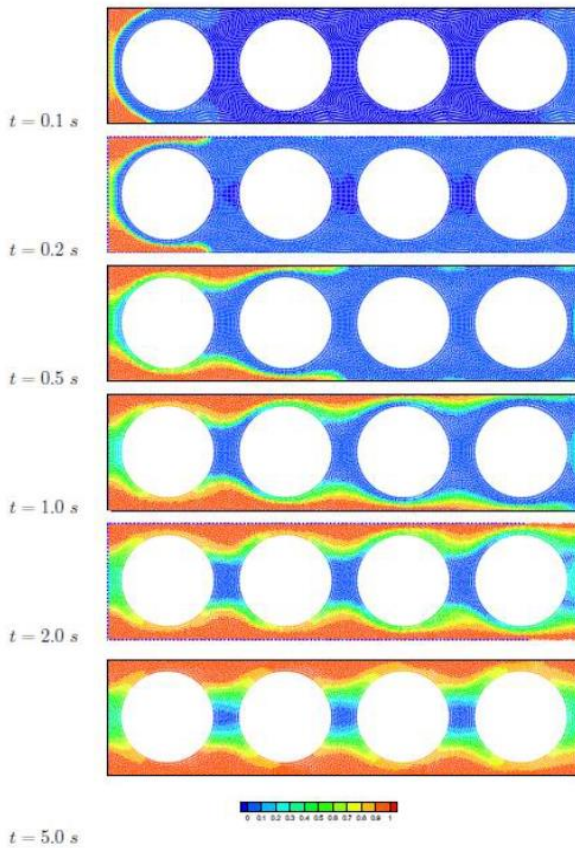


Figure 4. The results of normalized concentration of asphaltene for different times

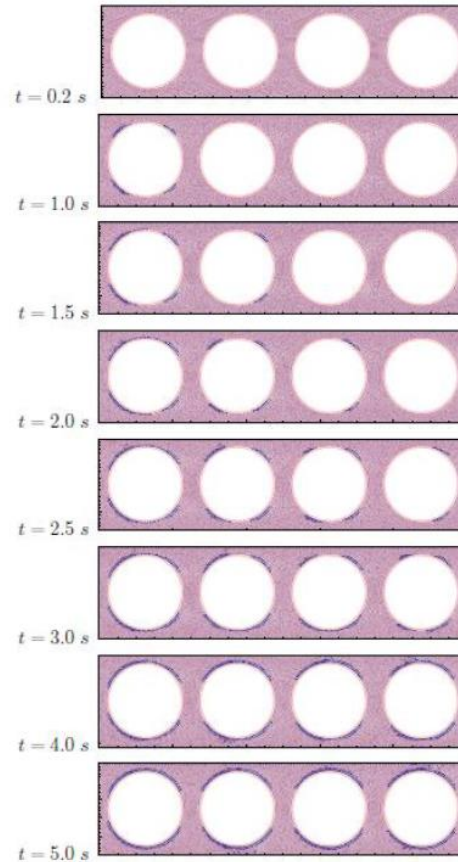


Figure 5. The results of asphaltene flocs precipitation during time. (Dark particles represent asphaltene deposits.)

In early times, two channels are formed up and down the grain, and the fluid preferred to flow through these channels. Thus, the domain can be divided into high-speed regions, i.e., these channels and low-speed regions which include the spaces between the grains in the middle of the domain horizontally. In high-speed regions, the dominant effect is advection while in the latter diffusion effect is more significant.

At  $t = 1.0$  s the front of injected fluid reaches the outlet boundary, and after that, the diffusion effect extends the influenced region to the whole domain slowly.

The particles near the walls have a chance to be deposited because of their low velocity if their concentration were higher than the critical value  $C_{cr}$ . In this simulation,  $C_{cr}$  was selected as  $0.5 C_{in}$ . Figure 5 indicates the amount of deposited SPH particles in the numerical results by dark dots. In this figure, it can be seen that after a certain time asphaltene flocs concentration of the particles near the wall of the first grain reaches the critical value  $C_{cr}$  and they settle down. For more clarity, the above results are also shown in Figure 6 for the first grain (periodic cell). In this figure, in addition, velocity vectors of the SPH particles are illustrated. It can be seen that in the earlier time ( $t \leq 2$ ) asphaltene flocs gradually settle on the surface of the grain. Then, it develops a stable layer. After this time, any floc added to the deposited layer is removed by the shear stress of the flowing fluid. The same phenomenon occurs for the other gains with a certain delay, which can be recognized in Figure 5.

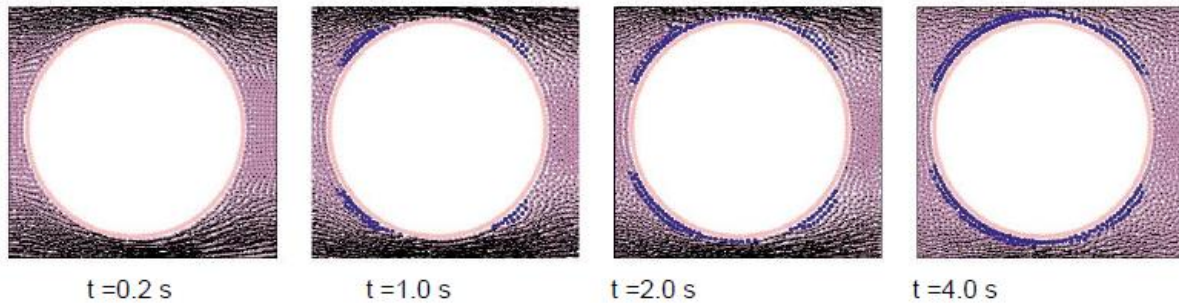


Figure 6. Particles distributions and velocity vectors for four different times around the first grain. (Dark particles represent asphaltene deposits.)

### 5. Modeling and discussion

To determine the permeability change using the results of numerical simulations one should average the velocity field  $V$  over the spatial domain to obtain Darcy's velocity  $u$  which in the discrete form is,

$$u = \phi \frac{\sum_i^N V_i \omega_i}{\sum_i^N \omega_i} \tag{12}$$

where  $\phi$  is the porosity of medium, which in this case is equal  $1 - \pi D^2/4s^2 = 0.50$ . Then Darcy's law for the averaged volume reads

$$K = \frac{u_x \mu}{\rho g} \tag{13}$$

where  $u_x$  is the  $x_i$  component of Darcy's velocity, and  $K$  is the (absolute) permeability.

#### 5.1. Permeability change for a single cell

The above procedure was done for the obtained numerical results of the previous section for every time-step, and the resulted permeability is plotted versus time in Figure 7. To better show the evolution of the permeability, in this figure, it is normalized by using the initial value of the permeability of the medium  $K_{init}$ .

In Figure 7, three regions can be recognized. The schematic diagram of these regions (based on Figure 7) is shown in Figure 8 for an arbitrary periodic cell in the medium. In the first region (I), no precipitation has been formed. In this region, the local permeability of the intended cell is constant, and it is equal to the initial permeability of the medium  $K_{init}$  in single-

phase flow of oil. At a certain time  $t_i$ , the precipitation of asphaltene is begun. Here, it is denoted as the onset of permeability changes.

The local permeability in the region (II) is strictly descending. The rate of this process decreases as the time passes. The reason is the increase in velocity caused by decreasing the cross-section of flow. It also causes some deposited flocs to be removed from the surface of the grains. Therefore, after a certain time ( $\tau$ ) the asphaltene precipitation process will be stable.

Consequently, the net rate of precipitation will be zero. In this state, the flow in the considered cell becomes steady. Then, the region (III) is begun. In this region, the local permeability is constant and equal to  $K_{fin}$ .

It must be mentioned that the above behavior occurs under conditions when the flow rate is kept constant. Otherwise, the third region is not formed. Meanwhile, it is likely that the porous media become blocked completely. In addition, in the constant flow rate conditions it is concluded that for one alternative media the parameters in Figure 8.  $\tau$ ,  $K_{init}$  and  $K_{fin}$  are almost the same for all cells. Their difference is only the time of beginning the second region  $t_i$ . Let consider the normalized permeability for the cell  $i$  be  $K_i/K_{init} = f_i(t)$ . Then

$$\frac{K_i}{K_{init}} = f_{i-1}(t - \Delta t) = f_0(t - i\Delta t) \tag{14}$$

where  $f_0(t)$  is the permeability change function for the first grain (cell). It is supposed that  $t_0 = 0$ . In addition,  $\Delta t$  is the time between the onsets of permeability change for two adjacent cells, i.e.,  $\Delta t = t_i - t_{i-1}$ . Note, the difference between  $\tau$  and  $\Delta t$ . The value of  $\Delta t$  may be assumed to be equal to the time it takes for the flow to pass through a cell. That is  $\Delta t = s/u_x$ . A suitable relation, which fits well with the aforementioned model, is

$$\frac{K_i}{K_{init}} = \left( 1 + \frac{K_i - K_{init}}{2} \left( 1 + \tanh \left( \alpha \left( 2 \frac{t - t_i}{\tau} - 1 \right) \right) \right) \right)^{-1} \tag{15}$$

where  $\alpha$  is a tuning parameter which is set here to 3. For the numerical results in Figure 7 and the other parameters are  $K_{fin}/K_{init} = 0.17$  and  $\tau = 5$  s.

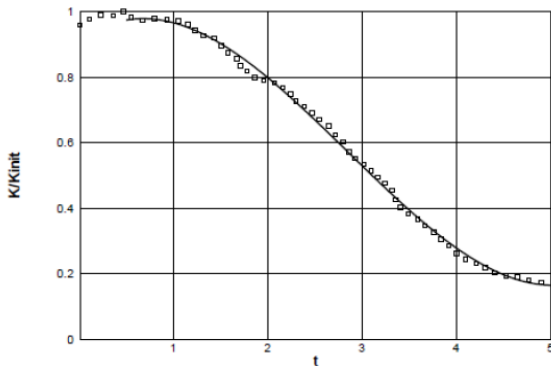


Figure 7. Fraction of absolute permeability to the initial permeability versus time

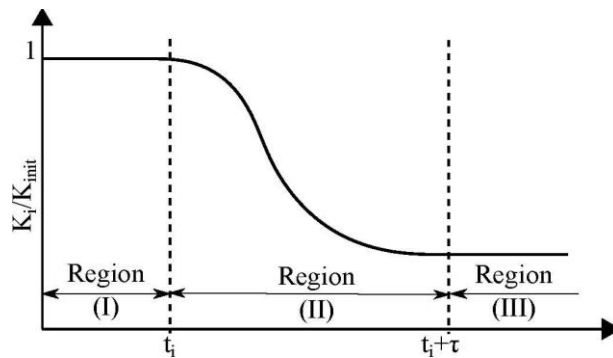


Figure 8. Schematic diagram for normalized permeability changes in time for a periodic cell  $i$

### 5.2. Permeability change for a slim tube

The above model is appropriate for only one cell in the medium. For a slim tube with numerous grain arranged in series, the permeability of each cell at a certain time should be averaged. In the following, an averaging process is presented to obtain a model for the permeability change for a slim tube based on the numerical results and modeling of the previous sections.

If  $K_n(t)$  is the average permeability of a porous medium including  $n$  periodic cells and since the cells are series it follows:

$$\frac{1}{\bar{K}_n(t)} = \frac{1}{nK_{init}} \sum_{i=0}^{n-1} \frac{1}{K_i(t)} = \frac{1}{nK_{init}} \sum_{i=0}^{n-1} \frac{1}{f_i(t)} \tag{16}$$

Regarding the periodic property of  $f(t)$  in Eq. (14) the sum in Eq. (16) can be rewritten as one integral approximation as

$$\frac{K_{init}}{K_n(t)} = \frac{1}{n\Delta t} \int_0^{n\Delta t} \frac{dt}{f_0(t-t)} \tag{17}$$

where  $K_{init}$  is also the initial permeability of the slim tube. Then by replacing the value of  $\Delta t = s/u_x$  and changing the variable one has

$$\frac{K_n(t)}{K_{init}} \cong \frac{L}{u_x \int_{t-L/ux}^t \frac{d\eta}{f_0(\eta)}} \tag{18}$$

in which  $L = n_s$  is the length of the tube. By defining

$$T(t) = \int_0^t \frac{d\eta}{f_0(\eta)} \tag{19}$$

Eq. (18) can be simplified as,

$$\frac{K_n(t)}{K_{init}} \cong \frac{T}{F(t)-F(t-T)} \tag{20}$$

where  $T = L/u_x$  is the time needed for the flow to pass through the slim tube. Now by substituting the new model presented in Eq. (15) for a cell in Eq. (20) one can conclude that

$$\frac{K_n(t)}{K_{init}} \cong \frac{1}{1 + \beta + \frac{\beta\tau}{2\alpha T} \ln \left( \frac{\cosh\left(\alpha\left(2\frac{t}{r}-1\right)\right)}{\cosh\left(\alpha\left(2\frac{t-T}{r}-1\right)\right)} \right)} \quad \text{where } \beta = \frac{K_{int}}{K_{fin}} - 1/2 \tag{21}$$

This equation simply relates the macro-scale average permeability of a slim tube to the pore-scale parameters  $K_{fin}/K_{init}$  and  $\tau$ .

Using this up-scaling process the macro-scale permeability reduction of a porous medium can be predicted using pore-scale data. For example, using the previous data of Figure 7 the permeability reduction plots of two "short" and "long" slim tubes with  $T = 100s$  and  $T = 500s$  are shown in Figure 9. In this figure, it is observable that for the "short" slim tube ( $T = 100s$ ) the permeability decreases during the time until the front of the injected asphaltene reaches the end of the tube ( $t = T$ ). After that, the whole tube is at a stable condition with deposited asphaltene, so the permeability reaches its final value  $K_{fin}$ .

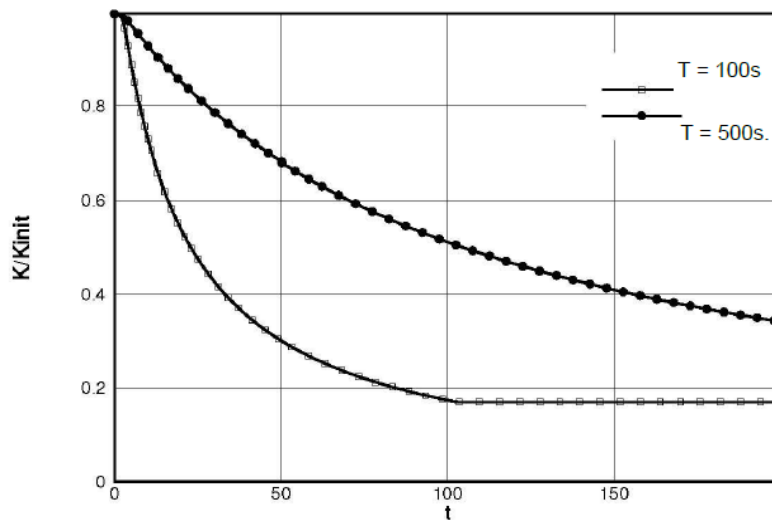


Figure 9. The results of permeability reduction of versus time based on the pore-scale simulation results for two slim tubes with  $T = 100s$  and  $T = 500s$

For the "long" slim tube ( $T = 500s$ ) (is shown in Figure 9), the time of the supposed experiment in Figure is not enough to reach the final stable condition. Thus, the permeability is strictly reducing during the experiment. This is more common in the real experiments. The same trend can be seen for instance in the works by Ashoori *et al.* [13] and Alizadeh *et al.* [14].

For such conditions in which  $\tau \ll t \ll T$  the Eq. (21) can be simplified more as

$$\frac{K_n(t)}{K_{init}} \cong \frac{1}{1 + \beta \frac{t}{T}} \quad \beta = \frac{K_{int}}{K_{fin}} - 1/2 \quad (22)$$

This relation has only two parameters  $\beta$  and  $L$  and the first parameter belongs to the pore-scale phenomena while the latter is just a property of the flow in the slim tube.

## 6. Conclusion

In the current work, asphaltene precipitation in the granular porous medium was simulated in pore scale using an improved version of the Lagrangian particle-based method SPH. Using the numerical results of pore-scale simulation a model for the permeability reduction versus time (Eq. (15)) was developed for a single grain (periodic cell). Based on this model and using an up-scaling process another relation (Eq. (21)) was presented which describes the evolution of the permeability of a slim tube during precipitation of asphaltene. The main outcomes of this study can be expressed as below.

The results of the SPH method in the pore-scale simulation properly show the physical behavior of the flow including asphaltene flocs concentration velocity and pressure fields. In a constant flow rate, a repeated phenomenon for each grain can be recognized in which a deposited layer is gradually developed and reaches the steady state.

- ✓ A hyperbolic function model (Eq. (15)) can describe the evolution of the permeability of a single grain (periodic cell) during precipitation of asphaltene. In this function, there are two parameters; final to initial permeability  $K_{fin}/K_{init}$  and characteristic time of precipitation  $\tau$  that should be evaluated through pore-scale simulation.
- ✓ By up scaling the model of a single grain the time evolution of the permeability of a slim tube or similar porous media is obtained. Here the suggested model (Eq. (21)) just needs the length of the tube and Darcy's velocity in addition to the aforementioned Pore-scale parameters.
- ✓ For enough long slim tubes, the model can be simplified to the form, which fits well with the laboratory experiments. The proposed models describe the permeability change with no need to know the changes of porosity.
- ✓ The developed model simulates the permeability reduction in flooding tests using computer code. The model provides good fit from the experimental data, which is an indication of the reliability of the developed model.

## References

- [1] Civan F. Scale effect on porosity and permeability: Kinetics, model, and correlation. *AICHE journal*, 2001; 47(2): 271-287.
- [2] Civan F. Modeling and simulation of formation damage by organic deposition, in: First international symposium in colloid chemistry in oil production: Asphaltenes and wax deposition. *JSCOP*, 1995: 26-29.
- [3] Civan F. Formation damage mechanisms and their phenomenological modeling -an overview. in: *European Formation Damage Conference*, Society of Petroleum Engineers, 2007.
- [4] Ali M, Islam M. The effect of asphaltene precipitation on carbonate-rock permeability: an experimental and numerical approach. *SPE production & facilities*, 1998; 13(3): 178-183.
- [5] Wang S, Civan F. Productivity decline of vertical and horizontal wells by asphaltene deposition in petroleum reservoirs, in: *SPE international symposium on oilfield chemistry*, Society of Petroleum Engineers, 2001.
- [6] Wang S, Civan F, Strycker, AR. Simulation of paraffin and asphaltene deposition in porous media, in: *SPE international symposium on oilfield chemistry*, 1999: 449-458.
- [7] Lucy LB. A numerical approach to the testing of the fission hypothesis. *The astronomical journal*, 1977; 82: 1013-1024.

- [8] Gingold RA, Monaghan JJ. Smoothed particle hydrodynamics: theory and application to non-spherical stars, *Monthly notices of the royal astronomical society*. 1977; 181(3): 375-389.
- [9] Monaghan JJ. Smoothed particle hydrodynamics. *Reports on progress in physics*, 2005; 68(8): 1703.
- [10] Fatehi R, Manzari M. A consistent and fast weakly compressible smoothed particle hydrodynamics with a new wall boundary condition. *International Journal for Numerical Methods in Fluids*, 2012; 68(7): 905-921.
- [11] Wendland H. Piecewise polynomial, positive definite and compactly supported radial functions of minimal degree. *Advances in computational Mathematics*, 1995; 4(1): 389-396.
- [12] Randles P, Libersky L. Smoothed particle hydrodynamics: some recent improvements and applications. *Computer methods in applied mechanics and engineering*, 1996; 139(1-4): 375-408.
- [13] Ashoori S, Manshad AK, Alizadeh N, Masoomi M, Tabatabaei S. Simulation and Experimental Investigation of the Permeability Reduction due to Asphaltene Deposition in Porous Media. *Iranian Journal of Chemical Engineering*, 2010: 3-16.
- [14] Alizadeh N, Khaksar Manshad A, Fadili A, Leung E, Ashoori S. Simulating the permeability reduction due to asphaltene deposition in porous media. in: *International Petroleum Technology Conference, International Petroleum Technology Conference*, 2009.
- [15] Manshad AK, Manshad MK, Ashoori S. The application of an artificial neural network (ANN) and a genetic programming neural network (GPNN) for the modeling of experimental data of slim tube permeability reduction by asphaltene precipitation in Iranian crude oil reservoirs. *Petroleum Science and Technology*, 2012; 30(23): 2450-2459.
- [16] Manshad AK, Mofidi AM, Shariatpanahi F, Edalat M. Developing of scaling equation with function of pressure to determine onset of asphaltene precipitation. *Journal of the Japan Petroleum Institute*, 2018; 51(2): 102-106.

---

*To whom correspondence should be addressed: Dr. Amir H Mohammadi, Discipline of Chemical Engineering, School of Engineering, University of KwaZulu-Natal, Howard College Campus, Durban 4041, South Africa, E-mail: [amir\\_h\\_mohammadi@yahoo.com](mailto:amir_h_mohammadi@yahoo.com) and Dr. Abbas Khaksar Manshad, Department of Petroleum Engineering, Abadan Faculty of Petroleum Engineering, Petroleum University of Technology (PUT), Abadan, Iran, Email: [khaksar@put.ac.ir](mailto:khaksar@put.ac.ir)*